1 **Increased lung cell entry of B.1.617.2 and evasion of antibodies induced by**

2 **infection and BNT162b2 vaccination**

3

4 **Prerna Arora[1,2], Amy Kempf[1,2], Inga Nehlmeier[1], Anzhalika Sidarovich[1,2], Nadine Krüger[1],**

5 **Luise Graichen[1,2], Anna-Sophie Moldenhauer[1], Martin S. Winkler[3], Sebastian Schulz[4],**

6 **Hans-Martin Jäck[4], Metodi V. Stankov[5], Georg M. N. Behrens[5], Stefan Pöhlmann[1,2,*],**

7 **Markus Hoffmann[1,2,*]**

8

9 [1]Infection Biology Unit, German Primate Center, Kellnerweg 4, 37077 Göttingen, Germany

10 [2]Faculty of Biology and Psychology, Georg-August-University Göttingen, Wilhelmsplatz 1,

11 37073 Göttingen, Germany

12 [3]Department of Anaesthesiology, University of Göttingen Medical Center, Göttingen, Georg-

13 August University of Göttingen, Robert-Koch-Straße 40, 37075 Göttingen, Germany

14 [4] Division of Molecular Immunology, Department of Internal Medicine 3, Friedrich-Alexander

15 University of Erlangen-Nürnberg, Glückstraße 6, 91054 Erlangen, Germany

16 [5] Department for Rheumatology and Immunology, Hannover Medical School, Carl-Neuberg-Str.

17 1, 30625 Hannover, Germany

18

19 *E-mail: mhoffmann@dpz.eu (M.H.), spoehlmann@dpz.eu (S.P.)

20

21

22

23

24

SUMMARY

The delta variant of SARS-CoV-2, B.1.617.2, emerged in India and has subsequently spread to over 80 countries. B.1.617.2 rapidly replaced B.1.1.7 as the dominant virus in the United Kingdom, resulting in a steep increase in new infections, and a similar development is expected for other countries. Effective countermeasures require information on susceptibility of B.1.617.2 to control by antibodies elicited by vaccines and used for COVID-19 therapy. We show, using pseudotyping, that B.1.617.2 evades control by antibodies induced upon infection and BNT162b2 vaccination, although with lower efficiency as compared to B.1.351. Further, we found that B.1.617.2 is resistant against Bamlanivimab, a monoclonal antibody with emergency use authorization for COVID-19 therapy. Finally, we show increased Calu-3-lung cell entry and enhanced cell-to-cell fusion of B.1.617.2, which may contribute to augmented transmissibility and pathogenicity of this variant. These results identify B.1.617.2 as an immune evasion variant with increased capacity to enter and fuse lung cells.

49 **INTRODUCTION**

50 Vaccines based on inactivated whole virus, adenoviral vectors or mRNAs encoding the severe

51 acute respiratory syndrome coronavirus 2 (SARS-CoV-2) spike (S) protein protect against

52 coronavirus disease 2019 (COVID-19) and allow to effectively combat the COVID-19 pandemic

53 (Polack et al., 2020, Golob et al., 2021, Xia et al., 2021). These vaccines present the S proteins of

54 viruses circulating early during the pandemic as antigens to the immune system. However, at a

55 later stage of the pandemic so called SARS-CoV-2 variants of concern (VOC) emerged that

56 harbor mutations in the S protein that allow for augmented transmissibility (B.1.1.7, alpha

57 variant) and/or immune evasion (B.1.351, beta variant; P.1, gamma variant) (Plante et al., 2021b).

58 Mutations conferring increased transmissibility might augment binding to the cellular receptor

59 ACE2 while mutations conferring immune evasion alter epitopes of neutralizing antibodies

60 (Plante et al., 2021b). Immune evasion can allow for infection of convalescent or vaccinated

61 individuals but vectored and mRNA-based vaccines protect against severe COVID-19 induced by

62 alpha, beta and gamma VOC.

63 A massive surge of COVID-19 cases was detected in India between April and May 2021

64 and was associated with spread of a new variant, B.1.617, that subsequently branched off into

65 B.1.617.1, B.1.617.2 and B.1.617.3. The B.1.617.2 variant subsequently spread into more than 80

66 countries and became dominant in India and the United Kingdom(Singh et al., 2021, Campbell et

67 al., 2021). In the UK, the spread of B.1.617.2 was associated with a marked increase in cases and

68 more than 80% of new infections are now due to B.1.617.2. A rapid increase of B.1.617.2 spread

69 is also expected in Germany, the US and several other countries, and a recent massive increase of

70 cases in Lisbon, Portugal, that required travel restrictions is believed to be due to B.1.617.2. In

71 order to contain spread of B.1.617.2, now considered a VOC, it will be critical to determine

72 whether convalescent or vaccinated patients are protected against infection by this variant. Here,

3

73   we addressed this question using reporter particles pseudotyped with the SARS-CoV-2 spike (S)

74   protein, which are suitable tools to study SARS-CoV-2 neutralization by antibodies (Riepler et

75   al., 2020, Schmidt et al., 2020).

76

77

78

79

80

81

82

83

84

85

86

87

88

89

90

91

92

93

94

95

96

97 **RESULTS**

98   The S protein of B.1.617.2 harbors nine mutations in the surface unit, S1, of the S protein

99 and 1 mutation in the transmembrane unit, S2 (Figure 1A-B). Mutations T19R, G142D, E156G,

100 F157Δ and R158Δ are located in the N-terminal domain of S1, which contains epitopes for

101 neutralizing antibodies (Liu et al., 2020, McCallum et al., 2021, Suryadevara et al., 2021, Chi et

102 al., 2020). The receptor binding domain (RBD) harbors mutations L452R and T478K. Mutation

103 L452R reduces antibody-mediated neutralization (Deng et al., 2021, Liu et al., 2021b) and it has

104 been speculated that T478K might increase infectivity (Wang et al., 2021). Mutation D614G is

105 located between RBD and S1/S2 cleavage sites and linked to increased ACE2 binding,

106 replication in the upper respiratory tract and transmission (Figure 1A-B) (Plante et al., 2021a,

107 Zhou et al., 2021). Finally, P681R might increase cleavage of S protein at the S1/S2 site while the

108 impact of D950N on S protein driven entry and its inhibition by antibodies is unknown.

109   We first asked whether B.1.617.2 S protein mediates robust entry into cell lines frequently

110 used for SARS-CoV-2 research, Vero (African green monkey, kidney), 293T (human, kidney),

111 Caco-2 (human, colon) and Calu-3 (human, lung). All cell lines express endogenous ACE2 and

112 Vero, Caco-2 and Calu-3 cells are often used for infection studies with authentic SARS-CoV-2.

113 The B.1.617.2 S protein mediated entry into 293T and Vero cells with the same efficiency as WT

114 S protein while entry into Caco-2 (~1.5-fold) and Calu-3 cells (~2.0-fold) was augmented (Figure

115 1C and Supplemental figure 1A). The lung is the central target of SARS-CoV-2 but infection of

116 colon has also been reported, suggesting that B.1617.2 might have increased capacity to enter

117 target cells in these tissues. Finally, we did not detect increased ACE2 binding of B.1.617.2 S

118 protein (Figure 1D), suggesting that increased entry into Caco-2 and Calu-3 cells was not due to

119 augmented ACE2 binding.

120   Besides its ability to drive fusion of viral and cellular membranes, the S protein is further

121   able to drive the fusion of neighboring cells, resulting in the formation of multinucleated giant

122   cells, so called syncytia, which have been observed in vitro following directed S protein

123   expression or SARS-CoV-2 infection and in post mortem tissues from COVID-19 patients

124   (Bussani et al., 2020, Tian et al., 2020, Xu et al., 2020) . Since SARS-CoV-2 S protein-driven

125   syncytium formation is believed to contribute to COVID-19 pathogenesis, we investigated the

126   ability of B.1.617.2 S protein to drive cell-to-cell fusion in the human lung cell line A549, which

127   was engineered to express high levels of ACE2. As expected, directed expression of WT S led to

128   the formation of syncytia, while cells transfected with empty expression plasmid remained

129   normal (Figure 1E). Strikingly, directed expression of B.1.617.2 S protein caused more and larger

130   syncytia and quantification of cell-to-cell fusion revealed that fusion by B.1.617.2 S protein was

131   ~2.5-fold more efficient as compared to WT S (Figure 1E).

132   We next determined whether entry of B.1.617.2 is susceptible to inhibition by

133   recombinant antibodies with emergency use authorization for COVID-19 treatment. Three out

134   four antibodies tested inhibited B.1.617.2 S protein with similar efficiency as WT S protein

135   (Figure 1F and Supplemental figure 1C). However, B.1.617.2 was resistant to Bamlanivimab,

136   most likely because of mutation L452R (Supplemental figure 1B and (Starr et al., 2021)). Thus,

137   Bamlanivimab monotherapy is not suitable for prevention or treatment of B.1.617.2 infection.

138   Finally, we asked whether B.1.617.2 entry is inhibited by antibodies generated by infected or

139   vaccinated individuals. For these experiments, we employed the S protein of B.1.351 as control

140   since this VOC exhibits marked evasion from neutralizing antibodies. A previously described

141   collection of plasma (Hoffmann et al., 2021a) from convalescent COVID-19 patients collected at

142   University Hospital Göttingen, Germany, neutralized entry driven by B.1.617.2 S protein with

143   slightly reduced efficiency as compared to WT S protein (Figure 1G and Supplemental figure

144   1D). In contrast, neutralization of B.1.351 S protein-dependent entry was markedly reduced.

145   Finally, similar observations were made with previously characterized sera (Hoffmann et al.,

146   2021b) from donors who received two doses of BNT162b2, although immune evasion of

147   B.1.617.2. was more prominent as compared to convalescent sera (Figure 1H and Supplemental

148   figure 1E).

149

150

151

152

153

154

155

156

157

158

159

160

161

162

163

164

165

166

167

168 **DISCUSSION**

169   Our results demonstrate immune evasion, enhanced colon- and lung cell entry and

170   augmented syncytium formation by B.1.617.2. Evasion of antibody-mediated neutralization by

171   B.1.617.2 is in agreement with two recent studies (Liu et al., 2021a, Wall et al., 2021) and is

172   more prominent than previously observed by us for B.1.1.7 but less prominent as compared to

173   B.1.351 (Hoffmann et al., 2021a). This finding would be compatible with increased vaccine

174   breakthrough of B.1.617.2 but also suggests that BNT162b2 should still protect from B.1.617.2-

175   induced COVID-19. Treatment of infection with Bamlanivimab alone will be ineffective but we

176   expect that Casirivimab, Imdevimab and Etesevimab will be beneficial to B.1.617.2 infected

177   patients when administered early after infection. The observation that B.1.617.2 S protein is able

178   to cause more cell-to-cell fusion than WT S may suggest that B.1.617.2 could cause more tissue

179   damage, and thus be more pathogenic, than previous variants or that viral spread via syncytium

180   formation contributes to efficient inter- and intra-host spread of this variant. Entry experiments

181   with cell lines need to be interpreted with care and confirmation with primary cells is pending.

182   However, the significantly increased entry into the colon and lung cell lines Caco-2 and Calu-3,

183   respectively, suggest that B.1.617.2 might have an augmented capacity to infect these organs and

184   increased infection of the respiratory epithelium might account for the purported increased

185   transmissibility of B.1.617.2.

186

187

188

189

190

191

AUTHOR CONTRIBUTIONS

Conceptualization, M.H., S.P.; Funding acquisition, S.P.; Investigation, P.A., A.K., I.N., A.S., N.K., L.G., A.-S.M., M.H.; Essential resources, M.S.W., S.S., H.-M.J., M.V.S., G.M.N.B.; Writing, M.H., S.P.; Review and editing, all authors.

COMPETING INTERESTS

The authors declare no competing interests

216   **MATERIALS AND METHODS**

217

218   **Cell culture**

219   All cell lines were incubated at 37 °C in a humidified atmosphere containing 5% CO_2. 293T

220   (human, female, kidney; ACC-635, DSMZ, RRID: CVCL_0063), Vero76 cells (African green

221   monkey kidney, female, kidney; CRL-1586, ATCC; RRID: CVCL_0574, kindly provided by

222   Andrea Maisner) and BHK-21 (Syrian hamster, male, kidney; ATCC Cat# CCL-10; RRID:

223   CVCL_1915, kindly provided by Georg Herrler) and A549-ACE2 cells (Hoffmann et al., 2021a),

224   which were derived from parental A549 cells (human, male, lung; CRM-CCL-185, ATCC,

225   RRID:CVCL_0023; kindly provided by Georg Herrler), were cultured in Dulbecco's modified

226   Eagle medium (PAN-Biotech) supplemented with 10% fetal bovine serum (FBS, Biochrom), 100

227   U/ml penicillin and 0.1 mg/ml streptomycin (pen/strep) (PAN-Biotech). In addition, Calu-3

228   (human, male, lung; HTB-55, ATCC; RRID: CVCL_0609, kindly provided by Stephan Ludwig)

229   and Caco-2 cells (human, male, colon; HTB-37, ATCC, RRID: CVCL_0025) were cultured in

230   minimum essential medium (GIBCO) supplemented with 10% FBS, 1% pen/strep, 1x non-essential

231   amino acid solution (from 100x stock, PAA) and 1 mM sodium pyruvate (Thermo Fisher

232   Scientific). Cell lines were validated by STR-typing, amplification and sequencing of a fragment

233   of the cytochrome c oxidase gene, microscopic examination and/or according to their growth

234   characteristics. Furthermore, all cell lines were routinely tested for contamination by mycoplasma

235   contamination.

236

237   **Expression plasmids**

238   Plasmids encoding pCAGGS-DsRed, pCAGGS-VSV-G (vesicular stomatitis virus glycoprotein),

239   pCG1-WT SARS-CoV-2 S (codon optimized, based on the Wuhan/Hu-1/2019 isolate, equipped

10

240   with D614G mutation; with C-terminal truncation of the last 18 amino acid), pCG1-SARS-CoV-2

241   S, B.1.351 (codon optimized; with C-terminal truncation of the last 18 amino acid), ACE2

242   (angiotensin converting enzyme 2) and soluble ACE2 have been previously described (Hoffmann

243   et al., 2021a, Hoffmann et al., 2021b, Hoffmann et al., 2020). In order to generate the expression

244   vector for the S protein of SARS-CoV-2 variant B.1.617.2, the respective mutations were inserted

245   into the WT SARS-CoV-2 S sequence by splice-overlap PCR. The resulting open reading frame

246   was further inserted into vector pCG1 plasmid (kindly provided by Roberto Cattaneo, Mayo

247   Clinic College of Medicine, Rochester, MN, USA), using BamHI and XbaI restriction enzymes.

248   The integrity of all sequences was confirmed by sequence analysis using a commercial

249   sequencing service (Microsynth SeqLab). Specific details on the cloning procedure can be

250   obtained upon request. Transfection of 293T cells was carried out by the calcium-phosphate

251   precipitation method, while BHK-21 and A549-ACE2 cells were transfected using Lipofectamine

252   LTX (Thermo Fisher Scientific).

253

Sequence analysis and protein models

254

255   The S protein sequence of SARS-CoV-2 S variant B.1.617.2 (GISAID Accession ID:

256   EPI_ISL_1921353) was obtained from the GISAID (global initiative on sharing all influenza data)

257   databank (https://www.gisaid.org/). Protein models were generated employing the YASARA

258   software (http://www.yasara.org/index.html) and are based on published crystal structure PDB:

259   6XDG (Hansen et al., 2020), PDB: 7L3N (Jones et al., 2020) or PDB: 7C01 (Shi et al., 2020), or a

260   template that was constructed by modelling the SARS-2 S sequence on PDB: 6XR8 (Cai et al.,

261   2020), using the SWISS-MODEL online tool (https://swissmodel.expasy.org)

262

Production of pseudotype particles

263

264 Rhabdoviral pseudotypes bearing SARS-CoV-2 spike protein were generated according to an

265 established protocol (Berger Rentsch and Zimmer, 2011). Briefly, 293T cells were transfected with

266 expression plasmids encoding S protein, VSV-G or empty plasmid (control). At 24 h

267 posttransfection, cells were inoculated with a replication-deficient vesicular stomatitis virus that

268 lacks the genetic information for VSV-G and instead codes for two reporter proteins, enhanced

269 green fluorescent protein and firefly luciferase (FLuc), VSV∗ΔG-FLuc (kindly provided by Gert

270 Zimmer) at a multiplicity of infection of 3. Following 1 h of incubation at 37 °C, the inoculum was

271 removed and cells were washed with phosphate-buffered saline (PBS). Subsequently, cells

272 received culture medium containing anti-VSV-G antibody (culture supernatant from I1-hybridoma

273 cells; ATCC no. CRL-2700; except for cells expressing VSV-G, which received only medium) in

274 order to neutralize residual input virus. After 16-18h, the culture supernatant was harvested,

275 clarified from cellular debris by centrifugation at 4,000 x g, 10 min, aliquoted and stored at -80 °C.

276

Transduction of target cells

277

278 For transduction experiments, target cells were seeded in 96-well plates and inoculated with equal

279 volumes of pseudotype particles. The transduction efficiency was evaluated at 16-18 h post

280 transduction. For this, cells were lysed in PBS containing 0.5% triton X-100 (Carl Roth) for 30 min

281 at RT. Afterwards, cell lysates were transferred into white 96-well plates and mixed with luciferase

282 substrate (Beetle- Juice, PJK) before luminescence was recorded using a Hidex Sense Plate

283 luminometer (Hidex).

284

Analysis of ACE2 binding

For the production of soluble ACE2 fused to the Fc portion of human immunoglobulin G (IgG), sol-ACE2, 293T cells were seeded in a T-75 flask and transfected with 20 µg of sol-ACE2 expression plasmid. The medium was replaced at 10 h posttransfection and cells were further incubated for 38 h. Further, the culture supernatant was harvested and clarified by centrifugation at 2,000 x g, 10 min, 4 °C. Next, the clarified supernatant was loaded onto Vivaspin protein concentrator columns (molecular weight cut-off of 30 kDa; Sartorius) and centrifuged at 4,000 x g at 4 °C until the supernatant was 100-fold concentrated. Finally, concentrated sol-ACE2 was aliquoted and stored at -80 °C.

In order to test the binding efficiency of sol-ACE2 to S protein, BHK-21 cells were seeded in 12-well plates and transfected with expression plasmid for WT or SARS-CoV-2 S variant. Untransfected cells and cells transfected with empty pCG1 plasmid served as controls. At 24 h posttransfection, the culture supernatant was removed and cells were washed and resuspended in PBS and transferred into 1.5 ml reaction before being pelleted by centrifugation (600 x g, 5 min, RT, all centrifugation steps). Thereafter, cells were washed with PBS containing 1% bovine serum albumin (BSA; PBS/BSA) and pelleted again by centrifugation. Next, the supernatant was removed and cell pellets were incubated with 100 µl of solACE2-Fc (1:100 in PBS/BSA) and rotated for 1 h at 4 °C using a Rotospin eppi rotator disk (IKA). After incubation, cells were pelleted and incubated with 100 µl of human AlexaFlour-488-conjugated antibody (1:200 in PBS/BSA; Thermo Fisher Scientific) and rotated again as described above. Finally, cells were washed and resuspended in PBS/BSA and subjected to flow cytometry using a LSR II flow cytometer and the FACS diva software (BD Biosciences). Data analysis was performed using the FCS express 4 Flow research software (De Novo Software) in order to obtain the geometric mean values.

13

308

309   **Syncytium formation assay**

310   In order to analyze S protein-driven cell-to-cell fusion, A549-ACE2 cells were grown in 12-well

311   plates and transfected with expression vector for WT or B.1.617.2 S protein. In addition, cells

312   transfected with empty plasmid served as control. At 24 h posttransfection, cells were washed with

313   PBS and fixed by incubation (20 min, room temperature) with 4% paraformaldehyde solution (Carl

314   Roth). Thereafter, cells were washed with deionized water, air-dried and stained with May-

315   Gruenwald solution (30 min, room temperature; Sigma-Aldrich). Next, cells were washed three

316   times with deionized water, air-dried and 1:10 diluted Giemsa (30 min, room temperature; Sigma-

317   Aldrich) solutions. Finally, cells were washed three times with deionized water, air-dried and

318   analyzed by bright-field microscopy using a Zeiss LSM800 confocal laser scanning microscope

319   and the ZEN imaging software (Zeiss). For each sample, three randomly selected areas were

320   imaged and S protein-driven syncytium formation was quantified by counting the total number of

321   nuclei in syncytia per image. Syncytia were defined as cells containing at least three nuclei. To

322   eliminate potential bias and correct for counting errors, counting was performed blinded by two

323   persons independently and for each sample average counts were used. Further, for each biological

324   replicate, the average (mean) total number of nuclei in syncytia per image was calculated from

325   three images obtained for randomly selected areas of the well.

326

327   **Collection of serum and plasma samples**

14

328   Before analysis, all serum and plasma samples were heat-inactivated at 56 °C for 30 min. Further,

329   all plasma/serum samples were pre-screened for their ability to neutralize transduction of Vero

330   cells by pseudotype particles bearing WT SARS-CoV-2 S.

331   Convalescent plasma was obtained from COVID-19 patients treated at the intensive care unit of

332   the University Medicine Göttingen (UMG) under approval given by the ethic committee of the

333   UMG (SeptImmun Study 25/4/19 Ü). Cell Preparation Tube (CPT) vacutainers with sodium citrate

334   were used for collection of convalescent plasma. Further, plasma was collected as supernatant over

335   the peripheral blood mononuclear cell layer. In addition to convalescent plasma, serum from

336   individuals vaccinated with BioNTech/Pfizer vaccine BNT162b2/Comirnaty was collected 24-31

337   days after receiving the second dose using S-Monovette® EDTA tubes (Sarstedt). Sampling and

338   sample analysis were approved by the Institutional Review Board of Hannover Medical School

339   (8973_BO_K_2020, amendment Dec 2020).

340

341   **Neutralization assay**

342   For neutralization experiments, S protein bearing pseudotype particles were pre-incubated for 30

343   min at 37 °C with different concentrations of Casirivimab, Imdevimab, Bamlanivimab,

344   Etesevimab, or unrelated control IgG (2, 0.2, 0.02, 0.002, 0.0002, 0.00002 μg/ml). Alternatively,

345   pseudotype particles were pre-incubated with different dilutions (1:25, 1:100, 1:400, 1:1,600,

346   1:6,400) of convalescent plasma or serum from BNT162b2/Comirnaty vaccinated individuals.

347   Following incubation, mixtures were inoculated onto Vero cells with particles incubated only with

348   medium serving as control. Transduction efficiency was determined at 16-18 h postinoculation as

349   described above.

15

350

Data analysis

The results on S protein-driven cell entry represent average (mean) data acquired from six biological replicates, each conducted with four technical replicates. Data were normalized against WT S protein, for which entry was set as 1. Alternatively, transduction was normalized against the background signal (luminescence measured for cells inoculated with particles bearing no viral glycoprotein; set as 1). SolACE2 binding results are average (mean) data obtained from six biological replicates, each conducted with single samples. Each data point represents the geometric mean channel fluorescence for one biological replicate without normalization. Data on S protein-driven cell-to-cell fusion represent average (mean) data from four biological replicates, each conducted with single samples (three images per sample). Each data point represents the average (mean) number of nuclei in syncytia per image from two counting events by independent persons for each of the four biological replicate without normalization. The neutralization data are based on a single experiment (standard in the field), which were conducted with technical quadruplicates. For data normalized, background signals (Fluc signals obtained from cell inoculated with pseudotype particles bearing no S protein) were subtracted from all values and transduction by particles incubated only with medium was set as 0% inhibition. The neutralizing titer 50 (NT50) value, which indicates the plasma/serum dilution that causes a 50 % reduction of transduction efficiency, was calculated using a non-linear regression model (inhibitor vs. normalized response, variable slope).

Error bars are defined as either standard deviation (SD, neutralization data) or standard error of the mean (SEM, all other data). Data ware analyzed using Microsoft Excel (as part of the Microsoft Office software package, version 2019, Microsoft Corporation) and GraphPad Prism 8 version

16

373   8.4.3 (GraphPad Software). Statistical significance was tested by two-tailed Students t-test. Only p

374   values of 0.05 or lower were considered statistically significant (p > 0.05, not significant [ns]; p ≤

375   0.05, *; p ≤ 0.01, **; p ≤ 0.001, ***). Details on the statistical test and the error bars can be found

376   in the figure legends.

377

REFERENCES

BERGER RENTSCH, M. & ZIMMER, G. 2011. A vesicular stomatitis virus replicon-based bioassay for the rapid and sensitive determination of multi-species type I interferon. *PLoS One,* 6**,** e25858.

BUSSANI, R., SCHNEIDER, E., ZENTILIN, L., COLLESI, C., ALI, H., BRAGA, L., VOLPE, M. C., COLLIVA, A., ZANCONATI, F., BERLOT, G., SILVESTRI, F., ZACCHIGNA, S. & GIACCA, M. 2020. Persistence of viral RNA, pneumocyte syncytia and thrombosis are hallmarks of advanced COVID-19 pathology. *EBioMedicine,* 61**,** 103104.

CAI, Y., ZHANG, J., XIAO, T., PENG, H., STERLING, S. M., WALSH, R. M., JR., RAWSON, S., RITS-VOLLOCH, S. & CHEN, B. 2020. Distinct conformational states of SARS-CoV-2 spike protein. *Science,* 369**,** 1586-1592.

CAMPBELL, F., ARCHER, B., LAURENSON-SCHAFER, H., JINNAI, Y., KONINGS, F., BATRA, N., PAVLIN, B., VANDEMAELE, K., VAN KERKHOVE, M. D., JOMBART, T., MORGAN, O. & LE POLAIN DE WAROUX, O. 2021. Increased transmissibility and global spread of SARS-CoV-2 variants of concern as at June 2021. *Euro Surveill,* 26.

CHI, X., YAN, R., ZHANG, J., ZHANG, G., ZHANG, Y., HAO, M., ZHANG, Z., FAN, P., DONG, Y., YANG, Y., CHEN, Z., GUO, Y., ZHANG, J., LI, Y., SONG, X., CHEN, Y., XIA, L., FU, L., HOU, L., XU, J., YU, C., LI, J., ZHOU, Q. & CHEN, W. 2020. A neutralizing human antibody binds to the N-terminal domain of the Spike protein of SARS-CoV-2. *Science,* 369**,** 650-655.

DENG, X., GARCIA-KNIGHT, M. A., KHALID, M. M., SERVELLITA, V., WANG, C., MORRIS, M. K., SOTOMAYOR-GONZALEZ, A., GLASNER, D. R., REYES, K. R., GLIWA, A. S., REDDY, N. P., SANCHEZ SAN MARTIN, C., FEDERMAN, S., CHENG, J., BALCEREK, J., TAYLOR, J., STREITHORST, J. A., MILLER, S.,

402   SREEKUMAR, B., CHEN, P. Y., SCHULZE-GAHMEN, U., TAHA, T. Y., HAYASHI,

403   J. M., SIMONEAU, C. R., KUMAR, G. R., MCMAHON, S., LIDSKY, P. V., XIAO, Y.,

404   HEMARAJATA, P., GREEN, N. M., ESPINOSA, A., KATH, C., HAW, M., BELL, J.,

405   HACKER, J. K., HANSON, C., WADFORD, D. A., ANAYA, C., FERGUSON, D.,

406   FRANKINO, P. A., SHIVRAM, H., LAREAU, L. F., WYMAN, S. K., OTT, M.,

407   ANDINO, R. & CHIU, C. Y. 2021. Transmission, infectivity, and neutralization of a

408   spike L452R SARS-CoV-2 variant. *Cell*.

409 GOLOB, J. L., LUGOGO, N., LAURING, A. S. & LOK, A. S. 2021. SARS-CoV-2 vaccines: a

410   triumph of science and collaboration. *JCI Insight,* 6.

411 HANSEN, J., BAUM, A., PASCAL, K. E., RUSSO, V., GIORDANO, S., WLOGA, E.,

412   FULTON, B. O., YAN, Y., KOON, K., PATEL, K., CHUNG, K. M., HERMANN, A.,

413   ULLMAN, E., CRUZ, J., RAFIQUE, A., HUANG, T., FAIRHURST, J., LIBERTINY,

414   C., MALBEC, M., LEE, W. Y., WELSH, R., FARR, G., PENNINGTON, S.,

415   DESHPANDE, D., CHENG, J., WATTY, A., BOUFFARD, P., BABB, R.,

416   LEVENKOVA, N., CHEN, C., ZHANG, B., ROMERO HERNANDEZ, A., SAOTOME,

417   K., ZHOU, Y., FRANKLIN, M., SIVAPALASINGAM, S., LYE, D. C., WESTON, S.,

418   LOGUE, J., HAUPT, R., FRIEMAN, M., CHEN, G., OLSON, W., MURPHY, A. J.,

419   STAHL, N., YANCOPOULOS, G. D. & KYRATSOUS, C. A. 2020. Studies in

420   humanized mice and convalescent humans yield a SARS-CoV-2 antibody cocktail.

421   *Science,* 369**,** 1010-1014.

422 HOFFMANN, M., ARORA, P., GROSS, R., SEIDEL, A., HORNICH, B. F., HAHN, A. S.,

423   KRUGER, N., GRAICHEN, L., HOFMANN-WINKLER, H., KEMPF, A., WINKLER,

424   M. S., SCHULZ, S., JACK, H. M., JAHRSDORFER, B., SCHREZENMEIER, H.,

425   MULLER, M., KLEGER, A., MUNCH, J. & POHLMANN, S. 2021a. SARS-CoV-2

426   variants B.1.351 and P.1 escape from neutralizing antibodies. *Cell*.

427   HOFFMANN, M., HOFMANN-WINKLER, H., KRÜGER, N., KEMPF, A., NEHLMEIER, I.,

428   GRAICHEN, L., SIDAROVICH, A., MOLDENHAUER, A.-S., WINKLER, M. S.,

429   SCHULZ, S., JÄCK, H.-M., STANKOV, M. V., BEHRENS, G. M. N. & PÖHLMANN,

430   S. 2021b. SARS-CoV-2 variant B.1.617 is resistant to Bamlanivimab and evades

431   antibodies induced by infection and vaccination. *bioRxiv*, 2021.05.04.442663.

432   HOFFMANN, M., KLEINE-WEBER, H., SCHROEDER, S., KRUGER, N., HERRLER, T.,

433   ERICHSEN, S., SCHIERGENS, T. S., HERRLER, G., WU, N. H., NITSCHE, A.,

434   MULLER, M. A., DROSTEN, C. & POHLMANN, S. 2020. SARS-CoV-2 Cell Entry

435   Depends on ACE2 and TMPRSS2 and Is Blocked by a Clinically Proven Protease

436   Inhibitor. *Cell,* 181**,** 271-280 e8.

437   JONES, B. E., BROWN-AUGSBURGER, P. L., CORBETT, K. S., WESTENDORF, K.,

438   DAVIES, J., CUJEC, T. P., WIETHOFF, C. M., BLACKBOURNE, J. L., HEINZ, B. A.,

439   FOSTER, D., HIGGS, R. E., BALASUBRAMANIAM, D., WANG, L., BIDSHAHRI, R.,

440   KRAFT, L., HWANG, Y., ZENTELIS, S., JEPSON, K. R., GOYA, R., SMITH, M. A.,

441   COLLINS, D. W., HINSHAW, S. J., TYCHO, S. A., PELLACANI, D., XIANG, P.,

442   MUTHURAMAN, K., SOBHANIFAR, S., PIPER, M. H., TRIANA, F. J., HENDLE, J.,

443   PUSTILNIK, A., ADAMS, A. C., BERENS, S. J., BARIC, R. S., MARTINEZ, D. R.,

444   CROSS, R. W., GEISBERT, T. W., BORISEVICH, V., ABIONA, O., BELLI, H. M., DE

445   VRIES, M., MOHAMED, A., DITTMANN, M., SAMANOVIC, M., MULLIGAN, M. J.,

446   GOLDSMITH, J. A., HSIEH, C. L., JOHNSON, N. V., WRAPP, D., MCLELLAN, J. S.,

447   BARNHART, B. C., GRAHAM, B. S., MASCOLA, J. R., HANSEN, C. L. &

448   FALCONER, E. 2020. LY-CoV555, a rapidly isolated potent neutralizing antibody,

449   provides protection in a non-human primate model of SARS-CoV-2 infection. *bioRxiv*.

450   LIU, J., LIU, Y., XIA, H., ZOU, J., WEAVER, S. C., SWANSON, K. A., CAI, H., CUTLER,

451   M., COOPER, D., MUIK, A., JANSEN, K. U., SAHIN, U., XIE, X., DORMITZER, P. R.

452   & SHI, P. Y. 2021a. BNT162b2-elicited neutralization of B.1.617 and other SARS-CoV-2

453   variants. *Nature*.

454   LIU, L., WANG, P., NAIR, M. S., YU, J., RAPP, M., WANG, Q., LUO, Y., CHAN, J. F., SAHI,

455   V., FIGUEROA, A., GUO, X. V., CERUTTI, G., BIMELA, J., GORMAN, J., ZHOU, T.,

456   CHEN, Z., YUEN, K. Y., KWONG, P. D., SODROSKI, J. G., YIN, M. T., SHENG, Z.,

457   HUANG, Y., SHAPIRO, L. & HO, D. D. 2020. Potent neutralizing antibodies against

458   multiple epitopes on SARS-CoV-2 spike. *Nature,* 584**,** 450-456.

459   LIU, Z., VANBLARGAN, L. A., BLOYET, L. M., ROTHLAUF, P. W., CHEN, R. E.,

460   STUMPF, S., ZHAO, H., ERRICO, J. M., THEEL, E. S., LIEBESKIND, M. J.,

461   ALFORD, B., BUCHSER, W. J., ELLEBEDY, A. H., FREMONT, D. H., DIAMOND,

462   M. S. & WHELAN, S. P. J. 2021b. Identification of SARS-CoV-2 spike mutations that

463   attenuate monoclonal and serum antibody neutralization. *Cell Host Microbe,* 29**,** 477-488

464   e4.

465   MCCALLUM, M., DE MARCO, A., LEMPP, F. A., TORTORICI, M. A., PINTO, D., WALLS,

466   A. C., BELTRAMELLO, M., CHEN, A., LIU, Z., ZATTA, F., ZEPEDA, S., DI IULIO,

467   J., BOWEN, J. E., MONTIEL-RUIZ, M., ZHOU, J., ROSEN, L. E., BIANCHI, S.,

468   GUARINO, B., FREGNI, C. S., ABDELNABI, R., FOO, S. C., ROTHLAUF, P. W.,

469   BLOYET, L. M., BENIGNI, F., CAMERONI, E., NEYTS, J., RIVA, A., SNELL, G.,

470   TELENTI, A., WHELAN, S. P. J., VIRGIN, H. W., CORTI, D., PIZZUTO, M. S. &

471   VEESLER, D. 2021. N-terminal domain antigenic mapping reveals a site of vulnerability

472   for SARS-CoV-2. *Cell,* 184**,** 2332-2347 e16.

473   PLANTE, J. A., LIU, Y., LIU, J., XIA, H., JOHNSON, B. A., LOKUGAMAGE, K. G.,

474   ZHANG, X., MURUATO, A. E., ZOU, J., FONTES-GARFIAS, C. R.,

475   MIRCHANDANI, D., SCHARTON, D., BILELLO, J. P., KU, Z., AN, Z., KALVERAM,

476   B., FREIBERG, A. N., MENACHERY, V. D., XIE, X., PLANTE, K. S., WEAVER, S.

477   C. & SHI, P. Y. 2021a. Spike mutation D614G alters SARS-CoV-2 fitness. *Nature,* 592**,**

478   116-121.

479   PLANTE, J. A., MITCHELL, B. M., PLANTE, K. S., DEBBINK, K., WEAVER, S. C. &

480   MENACHERY, V. D. 2021b. The variant gambit: COVID-19's next move. *Cell Host*

481   *Microbe,* 29**,** 508-515.

482   POLACK, F. P., THOMAS, S. J., KITCHIN, N., ABSALON, J., GURTMAN, A., LOCKHART,

483   S., PEREZ, J. L., PEREZ MARC, G., MOREIRA, E. D., ZERBINI, C., BAILEY, R.,

484   SWANSON, K. A., ROYCHOUDHURY, S., KOURY, K., LI, P., KALINA, W. V.,

485   COOPER, D., FRENCK, R. W., JR., HAMMITT, L. L., TURECI, O., NELL, H.,

486   SCHAEFER, A., UNAL, S., TRESNAN, D. B., MATHER, S., DORMITZER, P. R.,

487   SAHIN, U., JANSEN, K. U., GRUBER, W. C. & GROUP, C. C. T. 2020. Safety and

488   Efficacy of the BNT162b2 mRNA Covid-19 Vaccine. *N Engl J Med,* 383**,** 2603-2615.

489   RIEPLER, L., ROSSLER, A., FALCH, A., VOLLAND, A., BORENA, W., VON LAER, D. &

490   KIMPEL, J. 2020. Comparison of Four SARS-CoV-2 Neutralization Assays. *Vaccines*

491   *(Basel),* 9.

492   SCHMIDT, F., WEISBLUM, Y., MUECKSCH, F., HOFFMANN, H. H., MICHAILIDIS, E.,

493   LORENZI, J. C. C., MENDOZA, P., RUTKOWSKA, M., BEDNARSKI, E., GAEBLER,

494   C., AGUDELO, M., CHO, A., WANG, Z., GAZUMYAN, A., CIPOLLA, M., CASKEY,

495   M., ROBBIANI, D. F., NUSSENZWEIG, M. C., RICE, C. M., HATZIIOANNOU, T. &

496   BIENIASZ, P. D. 2020. Measuring SARS-CoV-2 neutralizing antibody activity using

497   pseudotyped and chimeric viruses. *J Exp Med,* 217.

498   SHI, R., SHAN, C., DUAN, X., CHEN, Z., LIU, P., SONG, J., SONG, T., BI, X., HAN, C., WU,

499   L., GAO, G., HU, X., ZHANG, Y., TONG, Z., HUANG, W., LIU, W. J., WU, G.,

500   ZHANG, B., WANG, L., QI, J., FENG, H., WANG, F. S., WANG, Q., GAO, G. F.,

501   YUAN, Z. & YAN, J. 2020. A human neutralizing antibody targets the receptor-binding

502   site of SARS-CoV-2. *Nature,* 584**,** 120-124.

503   SINGH, J., RAHMAN, S. A., EHTESHAM, N. Z., HIRA, S. & HASNAIN, S. E. 2021. SARS-

504   CoV-2 variants of concern are emerging in India. *Nat Med*.

505   STARR, T. N., GREANEY, A. J., DINGENS, A. S. & BLOOM, J. D. 2021. Complete map of

506   SARS-CoV-2 RBD mutations that escape the monoclonal antibody LY-CoV555 and its

507   cocktail with LY-CoV016. *Cell Rep Med,* 2**,** 100255.

508   SURYADEVARA, N., SHRIHARI, S., GILCHUK, P., VANBLARGAN, L. A., BINSHTEIN,

509   E., ZOST, S. J., NARGI, R. S., SUTTON, R. E., WINKLER, E. S., CHEN, E. C.,

510   FOUCH, M. E., DAVIDSON, E., DORANZ, B. J., CHEN, R. E., SHI, P. Y.,

511   CARNAHAN, R. H., THACKRAY, L. B., DIAMOND, M. S. & CROWE, J. E., JR.

512   2021. Neutralizing and protective human monoclonal antibodies recognizing the N-

513   terminal domain of the SARS-CoV-2 spike protein. *Cell,* 184**,** 2316-2331 e15.

514   TIAN, S., HU, W., NIU, L., LIU, H., XU, H. & XIAO, S. Y. 2020. Pulmonary Pathology of

515   Early-Phase 2019 Novel Coronavirus (COVID-19) Pneumonia in Two Patients With

516   Lung Cancer. *J Thorac Oncol,* 15**,** 700-704.

517   WALL, E. C., WU, M., HARVEY, R., KELLY, G., WARCHAL, S., SAWYER, C., DANIELS,

518   R., HOBSON, P., HATIPOGLU, E., NGAI, Y., HUSSAIN, S., NICOD, J.,

519 GOLDSTONE, R., AMBROSE, K., HINDMARSH, S., BEALE, R., RIDDELL, A.,

520 GAMBLIN, S., HOWELL, M., KASSIOTIS, G., LIBRI, V., WILLIAMS, B.,

521 SWANTON, C., GANDHI, S. & BAUER, D. L. 2021. Neutralising antibody activity

522 against SARS-CoV-2 VOCs B.1.617.2 and B.1.351 by BNT162b2 vaccination. *Lancet,*

523 397**,** 2331-2333.

524 WANG, R., CHEN, J., GAO, K. & WEI, G. W. 2021. Vaccine-escape and fast-growing

525 mutations in the United Kingdom, the United States, Singapore, Spain, India, and other

526 COVID-19-devastated countries. *Genomics,* 113**,** 2158-2170.

527 XIA, S., ZHANG, Y., WANG, Y., WANG, H., YANG, Y., GAO, G. F., TAN, W., WU, G., XU,

528 M., LOU, Z., HUANG, W., XU, W., HUANG, B., WANG, H., WANG, W., ZHANG,

529 W., LI, N., XIE, Z., DING, L., YOU, W., ZHAO, Y., YANG, X., LIU, Y., WANG, Q.,

530 HUANG, L., YANG, Y., XU, G., LUO, B., WANG, W., LIU, P., GUO, W. & YANG, X.

531 2021. Safety and immunogenicity of an inactivated SARS-CoV-2 vaccine, BBIBP-CorV:

532 a randomised, double-blind, placebo-controlled, phase 1/2 trial. *Lancet Infect Dis,* 21**,** 39-

533 51.

534 XU, Z., SHI, L., WANG, Y., ZHANG, J., HUANG, L., ZHANG, C., LIU, S., ZHAO, P., LIU,

535 H., ZHU, L., TAI, Y., BAI, C., GAO, T., SONG, J., XIA, P., DONG, J., ZHAO, J. &

536 WANG, F. S. 2020. Pathological findings of COVID-19 associated with acute respiratory

537 distress syndrome. *Lancet Respir Med,* 8**,** 420-422.

538 ZHOU, B., THAO, T. T. N., HOFFMANN, D., TADDEO, A., EBERT, N., LABROUSSAA, F.,

539 POHLMANN, A., KING, J., STEINER, S., KELLY, J. N., PORTMANN, J., HALWE, N.

540 J., ULRICH, L., TRUEB, B. S., FAN, X., HOFFMANN, B., WANG, L., THOMANN, L.,

541 LIN, X., STALDER, H., POZZI, B., DE BROT, S., JIANG, N., CUI, D., HOSSAIN, J.,

542 WILSON, M. M., KELLER, M. W., STARK, T. J., BARNES, J. R., DIJKMAN, R.,

24

543   JORES, J., BENARAFA, C., WENTWORTH, D. E., THIEL, V. & BEER, M. 2021.

544   SARS-CoV-2 spike D614G change enhances replication and transmission. *Nature,* 592**,**

545   122-127.

546

547

548

549

550

551

552

553

554

555

556

557

558

559

560

561

562

563

564

565

566

567   **Figure legends**

568

569   **Figure 1: The spike protein of SARS-CoV-2 B.1.617.2 promotes efficient entry into human**

570   **lung and colon cells, causes more cell-to-cell fusion and evades from antibody-mediated**

571   **neutralization.**

572   (A) Schematic overview of the S protein from SARS-CoV-2 variant B.1.617.2 (RBD, receptor-

573   binding domain; TD, transmembrane domain).

574   (B) Location of the mutations found in SARS-CoV-2 variant B.1.617.2 in the context of the

575   trimeric spike protein (Color code: light blue, S1 subunit with RBD in dark blue; gray, S2

576   subunit; orange, S1/S2 and S2' cleavage sites; red, mutated amino acid residues).

577   (C) Pseudotyped particles bearing the S protein of wildtype (WT) SARS-CoV-2 or variant

578   B.1.617.2 were inoculated onto the indicated cell lines and transduction efficiency was quantified

579   by measuring virus-encoded luciferase activity in cell lysates at 16-18 h post transduction.

580   Presented are the average (mean) data from six biological replicates (each conducted with

581   technical quadruplicates) for which transduction was normalized against SARS-CoV-2 S WT (=

582   1). Error bars indicate the standard error of the mean. Statistical significance of differences

583   between WT and B.1.617.2 S proteins was analyzed by two-tailed Students t-test ($p > 0.05$, not

584   significant [ns]; $p \leq 0.01$, **). See also Figure S1A.

585   (D) BHK-21 expressing the S protein of WT SARS-CoV-2 or variant B.1.617.2 were

586   subsequently incubated with soluble ACE2 (harboring a C-terminal Fc-tag derived from human

587   IgG) and AlexaFluor-488-conjugated anti-human antibody, before being subjected to flow

588   cytometry. ACE2 binding efficiency was analyzed by measuring the geometric mean channel

589   fluorescence at 488 nm. Untransfected cells and cells transfected with empty expression plasmid

590   served as controls. Presented are the average (mean) data from six biological replicates (each

26

591   conducted with single samples). Error bars indicate the standard deviation (SD). Statistical

592   significance of differences between WT and variant B.1.617.2 S proteins was analyzed by two-

593   tailed Students t-test (p > 0.05, ns).

594   (E) Analysis of S protein induced cell-to-cell fusion. A549-ACE2 cells were transfected with

595   expression plasmid for the indicated S proteins or empty vector (EV). At 24 h posttransfection,

596   cells were fixed and subsequently stained with May-Gruenwald and Giemsa solutions.

597   Presented are representative microscopic images (scale bar = 200 µm). For quantification of

598   fusion efficiency, the total number of nuclei in syncytia per image was counted. Presented are the

599   average (mean) data from four biological replicates (each conducted with single samples; for

600   each sample, three randomly selected areas were imaged and independently analyzed by two

601   persons). Error bars indicate the SEM. Statistical significance of differences between WT and

602   B.1.617.2 S proteins was analyzed by two-tailed Students t-test (p ≤ 0.001, ***).
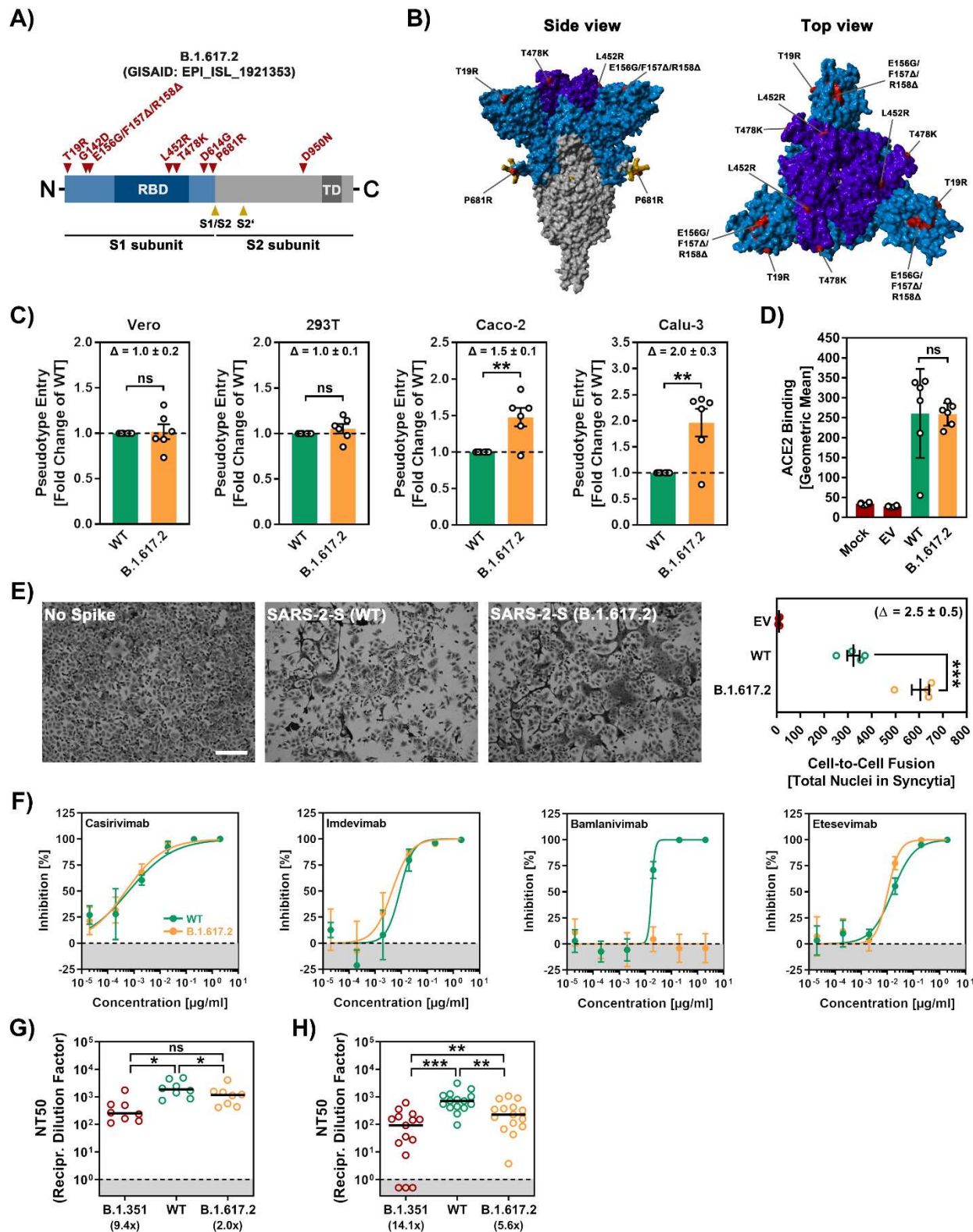
603   (F) Neutralization of SARS-CoV-2 WT, B.1.351 and B.1.617.2 S proteins by monoclonal

604   antibodies used for COVID-19 therapy. Pseudotyped particles bearing the S protein of WT

605   SARS-CoV-2 or variant B.1.617.2 were incubated for 30 min at 37 °C in the presence of

606   escalating concentrations (0.00002, 0.0002, 0.002, 0.02, 0.2, 2 µg/ml) of the indicated SARS-

607   CoV-2 S protein-specific monoclonal antibody (please see Figure S1B) or an unrelated control

608   antibody (please see Figure S1C), before being inoculated onto Vero cells. Transduction

609   efficiency was quantified by measuring virus-encoded luciferase activity in cell lysates at 16-18 h

610   post transduction. Presented are the average (mean) data from a single biological replicate

611   (conducted with technical quadruplicates) for which transduction was normalized against samples

612   that did not contain any antibody (= 0% inhibition). Error bars indicate the SD.

613   (G) Neutralization of SARS-CoV-2 WT, B.1.351 and B.1.617.2 S proteins by antibodies in

614   convalescent plasma. Pseudotyped particles bearing the S protein of WT SARS-CoV-2 or variant

27

615   B.1.617.2 were incubated for 30 min at 37 °C in the presence of different dilutions of

616   convalescent plasma (1:25, 1:100, 1:400, 1:1,600, 1:6,400, 1:25,600). Transduction efficiency

617   was quantified by measuring virus-encoded luciferase activity in cell lysates at 16-18 h post-

618   transduction and used to calculate the plasma dilution factor that leads to 50 % reduction in S

619   protein-driven cell entry (neutralizing titer 50, NT50). Presented are the data from a total of eight

620   convalescent plasma (black lines indicate the median). Statistical significance of differences

621   between the indicated groups was analyzed by two-tailed Students t-test ($p > 0.05$, ns; $p \leq 0.05$, *;

622     $p \leq 0.01$, **; $p \leq 0.001$, ***). Please see also Figure S1D.

623   (G) The experiment was performed as described for panel F but this time serum from

624   Comirnaty/BNT162b2-vaccinated individuals was investigated. Presented are the data from a

625   total of fifteen vaccinee sera (black lines indicate the median). Please see also Figure S1E.

626

627

628

629

630

631

632

633

634

635

636

637

638

28

Figure 1

639

1   **SI Figure Legend**

2

3   **Figure S1: Cell entry and evasion of antibody-mediated neutralization by the spike protein**

4   **of SARS-CoV-2 B.1.617.2 (related to Figure 1).**

5   (A) Transduction data normalized against the assay background (related to Figure 1C). The

6   experiment was performed as described in the legend of Figure 1C. Presented are the average

7   (mean) data from the same six biological replicates (each conducted with technical

8   quadruplicates) as presented in Figure 1C with the difference that transduction was normalized

9   against signals obtained from cells inoculated with particles bearing no viral glycoprotein

10   (background, set as 1). In addition, transduction data of particles bearing VSV-G are included.

11   Error bars indicate the SEM.

12   (B) Location of the receptor binding domain (gray) mutations L452R and T478K (both red) of

13   SARS-CoV-2 variant B.1.617.2 in the context of the interfaces for ACE2 binding (orange) and

14   binding of monoclonal antibodies used for COVID-19 therapy.

15   (C) An unrelated control antibody does not affect cell entry of pseudotype particles bearing

16   SARS-CoV-2 WT, B.1.351 or B.1.617.2 S (related to Figure 1E). The experiment was performed

17   as described in the legend of Figure 1E.

18   (D) Individual neutralization data for convalescent plasma (related to Figure 1F). Pseudotype

19   particles bearing the indicated S proteins were incubated (30 min, 37 °C) with different dilutions

20   of convalescent plasma before being inoculated onto Vero cells. Transduction efficiency was

21   quantified by measuring virus-encoded luciferase activity in cell lysates at 16-18 h

22   posttransduction. Presented are the data from a single representative experiment conducted with

23   technical quadruplicates. For normalization, inhibition of S protein-driven entry in samples

24   without plasma was set as 0%. Error bars indicate the SD. The data were further used to

25   calculated the plasma/serum dilution that leads to 50% reduction in S protein-driven cell entry

26   (neutralizing titer 50, NT50; shown in Figure 1F).

27   (E) Individual neutralization data for vaccinee serum (related to Figure 1G). Pseudotype particles

28   bearing the indicated S proteins were incubated (30 min, 37 °C) with different dilutions of serum

29   from individuals vaccinated with the Pfizer/BioNTech vaccine Comirnaty/BNT162b2 before

30   being inoculated onto Vero cells. Transduction efficiency was quantified by measuring virus-

31   encoded luciferase activity in cell lysates at 16-18 h posttransduction. Presented are the data from

32   a single representative experiment conducted with technical quadruplicates. For normalization,

33   inhibition of S protein-driven entry in samples without plasma was set as 0%. Error bars indicate

34   the SD. The data were further used to calculated the NT50 shown (shown in Figure 1G).

35

36

Figure S1

37

38